Supporting Information

Red Phosphorescent Binuclear Pt(Ⅱ) Complexes Incorporating bis(diphenylphorothioyl)amide Ligands: Synthesis, Photophysical Properties and Application in Solution Processible OLEDs

Xia Suo, [†a] Chuanli Nie, [†b] Weiqiang Liu, [c] Yuzhen Zhang, *[a] Yunjun Shen, *[a] Hedong Bian,*[a] and Gang Cheng*[c,d,e]

a. Guangxi Key Laboratory of Chemistry and Engineering of Forest Products, Guangxi Collaborative Innovation Center for Chemistry and Engineering of Forest Products, Guangxi University for Nationalities, Nanning 530006, China. E-mail: zhangyuzhen@gxun.edu.cn; yunjunshen@gxun.edu.cn; gxunchem@163.com

b. Guangxi Zhuang Autonomous Region Institute for the Prevention and Treatment of Occupational Diseases, Nanning 530021, China.

c. State Key Laboratory of Synthetic Chemistry, HKU-CAS Joint Laboratory on New Materials, and Department of Chemistry, The University of Hong Kong, Pokfulam Road, Hong Kong SAR, China, E-mail: ggcheng@hku.hk

d. HKU Shenzhen Institute of Research and Innovation, Shenzhen 518053, China

e. Hong Kong Quantum AI Lab Limited, 17 Science Park West Avenue, Pak Shek Kok, Hong Kong SAR

Xia Suo and Chuanli Nie contributed equally to this work.

Table of contents

General Information

All starting materials and ligand $L3H_2$ (1,4-diazanaphthalene) were purchased from commercial sources. Ligands bis(diphenylphosphorothioyl)amide (HStpip), and 2,5-bis(3-methylphenyl)pyrazine ($L1H_2$) were prepared following the previous report.[1-3] All chemical reagents are commercially available and can be used without further purification. The solvents used for synthesis were of analytical grade. All reactions requiring inert atmosphere were carried out using standard Schlenk techniques under dinitrogen. Deionized water (distilled water) was used throughout the experiment. ^{1}H and $^{13}C\{^{1}H\}$ NMR spectra were all recorded on Bruker 400 spectrometers. Chemical shifts (δ) are reported in parts per million (ppm) referenced to tetramethyl silane (δ 0.00) ppm using the residual protio solvent peaks as internal standards (^{1}H NMR experiments) or the characteristic resonances of the solvent nuclei (^{13}C NMR experiments). The coupling constant (J) is quoted in Hertz (Hz). The ^{13}C-NMR spectrum was recorded at a resonance frequency of 101.6 MHz. The following abbreviations are used to describe the multiplicity of signals: s (singlet); D (bimodal); t (triplet); Q (tetragonal); m (multimodal). High Resolution Mass spectra were run on a Thermo Q Exactive mass spectrometer. HRMS spectra for Pt(Stpip)L~3H and $Pt_2(Stpip)_2L$~3 $[M + H]^+$ were shown in Figure S4~9 (found, top; calculated, bottom). TLC analysis was performed on precoated silica gel thin layer chromatography plate GF254 slides and visualized by luminescence quenching either at (short wavelength) 254 nm or (long wavelength) 365 nm. Chromatographic purification of products was performed on a short column (length 30.0 cm, diameter 2.0 cm) using silica gel of 200−300 mesh using a forced flow of eluent. UV−vis absorption measurements were carried out on an Agilent's Cary 100 UV−vis spectrophotometer. Emission spectrum, phosphorescence lifetime and quantum yield were measured directly using Edinburgh Instruments model FLS1000. Emission spectra were acquired using xenon lamp excitation by exciting at the longest-wavelength absorption maxima with the excitation slit width 1.0 nm and emission slit width 1.0 nm. All samples for emission spectra were degassed by at least three freeze−pump−thaw cycles in an anaerobic cuvette and were pressurized with N_2 following each cycle. Luminescence quantum yields ϕ_{em} of the

complexes in solution were determined at 298 K (estimated uncertainty ±15%) using standard methods, and wavelength-integrated intensities (I) of the corrected emission spectra were compared to isoabsorptive spectra of quinine sulfate standard (ϕ_{ref} = 0.55 in 1 N H_2SO_4 air-equilibrated solution) and were corrected for solvent refractive index. Absolute quantum yields and phosphorescent lifetimes were measured in neat solid and thin films using an integrating sphere on the Edinburgh spectrophotometer FLS1000.. The radiative rate constant (k_r) and the nonradiative rate constant (k_{nr}) were estimated by using the following equations. [4]

$$QY = k_r \times \tau, \quad \tau = \frac{1}{k_r + k_{nr}}$$

Cyclic voltamograms were measured with CHI760e with a glassy carbon electrode (d = 2 mm) with a Pt counter electrode versus Ag^+/Ag reference electrode. The solvents used for measurement were of ACS grade.

Thermogravimetry Analysis. Thermogravimetric analysis (TGA) was carried out starting from room temperature (25 ℃) to 1000 ℃ (Pt(Stpip)L1H and $Pt_2(Stpip)_2L1$ to 800℃) at a heating rate of 10 ℃ / min in a N_2 atmosphere.

X-ray data collection and structure determination. The crystals of appropriate size were selected and placed on the Agilent Technologies single crystal diffractometer. Using graphite monochromatic MoKα rays (λ=0.71073Å), at a certain temperature, within a certain range of θ, the diffraction point data of the crystal is collected. Use the direct method and Olex2[5] and ShelXS[6] to solve the structure, and use ShelXL[7] for optimization. When mixing and adding hydrogen, hydrogen atoms use isotropic thermal parameters, and non-hydrogen atoms use anisotropic thermal parameters. The structure is corrected by the full matrix least square method. The thermal ellipsoid is set at the probability level of 30%. Molecular structures of Pt(Stpip)L1~3H $Pt_2(Stpip)_2L2$ and $Pt_{2(}Stpip)_2L3$ were shown in Figure2 and Figure S10 with a selective atomic numbering scheme. Thermal ellipsoids are drawn at the 30% probability level. The hydrogen atoms are omitted for clarity.

PMMA film: 1.00 mg of sample and 49.00 mg of polymethylmethacrylate (PMMA) were dissolved in 10 mL of dichloromethane solution. After mixing evenly, used a

dropper to take a little of the above solution and drop it evenly on quartz glass. After drying, a PMMA film containing sample can be obtained to measured its photophysical properties.

Experimental Section

Syntheses

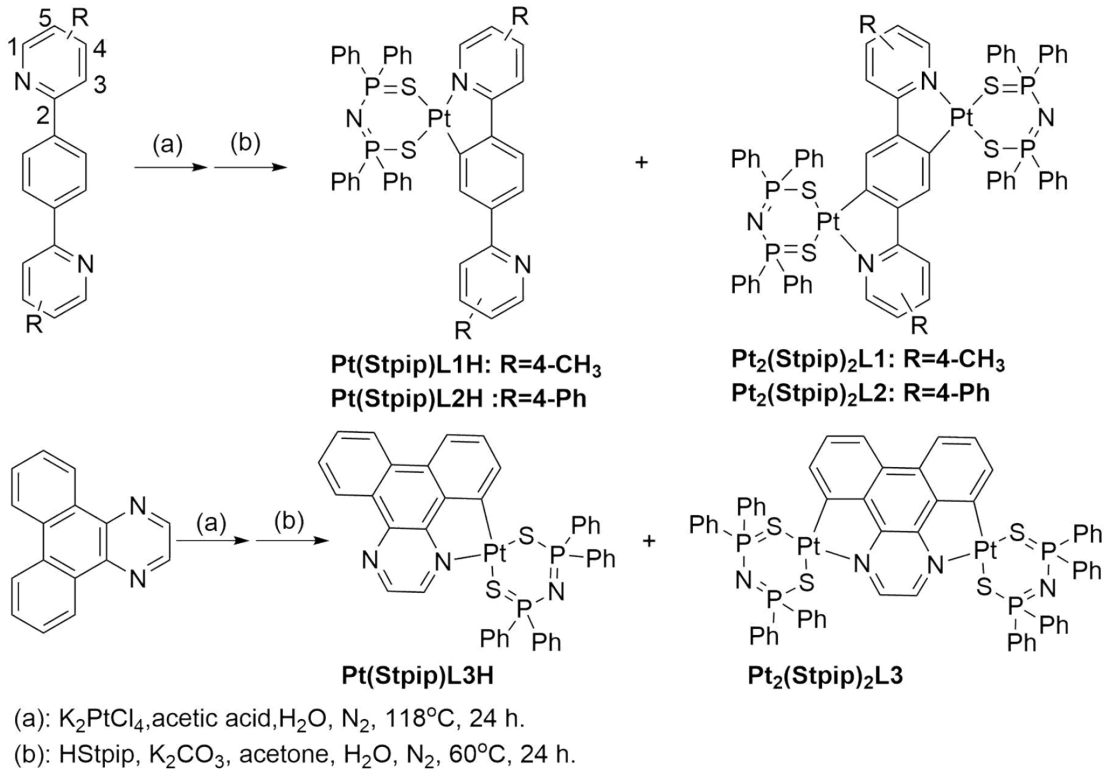

Figure S1. Synthesis of the ligands, binuclear complexes **Pt_2(Stpip)$_2$L1**, **Pt_2(Stpip)$_2$L2**, **Pt_2(Stpip)$_2$L3**, together with related mononuclear complexes **Pt(Stpip)L1H**, **Pt(Stpip)L2H**, **Pt(Stpip)L3H**.

L2H$_2$ 2,5-bis([1,1'-biphenyl]-3-yl)pyrazine: 1,4-biphenylboronic acid (1.04 g, 6.30 mmol) and 2-bromo-4-phenylpyridine (4.42 g, 18.9 mmol) were dissolved in 1,4-dioxane (50.0 mL). The mixture was deaerated by bubbling N_2 for 15 min, a solution of K_2CO_3 (1.80 g, 13.0 mmol) in water and $Pd(PPh_3)_4$ (1.31 g, 1.13 mmol) were then added. The mixture was degassed for a further 15 min. The mixture was refluxed for

24 hours under N_2. After cooling the reaction mixture to room temperature and removing all the solvents by rotary evaporation, CH_2Cl_2 was added. The organic layer was separated, washed with water, dried over $MgSO_4$, filtered, and evaporated to dryness. The crude product was purified by silica gel chromatography column with an eluent of Hexane/EtOAc (10:3). 1.84 g white solid was obtained (yield: 78%). ^{1}H NMR (400 MHz, $CDCl_3$, 25℃): 8.76 – 8.82 (d, J = 5.3 Hz, 2H), 8.22 – 8.27 (s, 4H), 8.02 – 8.07 (d, J = 1.8 Hz, 2H), 7.69 – 7.77 (m, 4H), δ 7.46 – 7.58 (m, 8H); ^{13}C NMR (100 MHz, $CDCl_3$, 25 ^{o}C): δ (ppm) =149.16 – 149.61, 129.47 – 129.71, 129.29 – 129.47, 127.68 – 127.93, 127.23 – 127.42, 120.77 – 121.01, 119.24 – 119.53.

Pt(Stpip)L1H and Pt_2(Stpip)$_2$L1. $L1H_2$ (0.0677 g, 0.26 mmol) was loaded into a Schlenk flask and pumped with vacuum for 10 min. After filling with N_2, degassed acetic acid (40.0 mL) and a solution of K_2PtCl_4 (0.216 g, 0.280 mmol) in water were transferred into the flask, respectively. After purging the mixture with N_2 for 20 min, the mixture was refluxed for 24 hours under N_2. The reaction mixture was cooled to room temperature, filtered, washed sequentially with acetic acid and ethanol, and dried to obtain dichlorobridged intermediate. The dichlorobridged intermediate (0.343, g, 0.529 mmol) and HStpip (0.53 g, 1.18 mmol) were loaded into a Schlenk flask and pumped with vacuum for 10 min. After filling with N_2, degassed acetone (73.0 mL) and a solution of K_2CO_3 (0.122 g, 8.83 mmol) in water were transferred into the flask, respectively. After purging the mixture with N_2 for 20 min, the mixture was refluxed for 24 hours under N_2. After cooling the reaction mixture to room temperature and removing all the solvents by rotary evaporation, CH_2Cl_2 was added. The organic layer was separated, washed with water, dried over $MgSO_4$, filtered, and evaporated to dryness. The crude product was purified by column chromatography with an eluent of CH_2Cl_2/Hexane (6:4) to obtain both the mononuclear and binuclear products.[8] **Pt(Stpip)L1H**: a yellow solid, 0.173 g, 26.8%. HRMS (ESI): m/z: 903.1443 $[M + H]^+$. Calcd for $C_{42}H_{36}N_3P_2PtS_2$ m/z 903.1468. **Pt_2(Stpip)$_2$L1**: an orange solid, 0.100 g, 15.5%. HRMS (ESI): m/z: 1544.1600 $[M + H]^+$. Calcd for $C_{66}H_{55}N_4P_4Pt_2S_4$ m/z 1544.1529.

Pt(Stpip)L2H and Pt_2(Stpip)$_2$L2. $L2H_2$ (0.100 g, 0.26 mmol) was loaded into a Schlenk flask and pumped with vacuum for 10 min. After filling with N_2, degassed acetic acid (40.0 mL) and a solution of K_2PtCl_4 (0.216 g, 0.280 mmol) in water were transferred into the flask, respectively. After purging the mixture with N_2 for 20 min, the mixture was refluxed for 24 hours under N_2. The reaction mixture was cooled to room temperature, filtered, washed sequentially with acetic acid and ethanol, and dried to obtain dichlorobridged intermediate. The dichlorobridged intermediate (0.409 g, 0.529 mmol), HStpip (0.53 g, 1.18 mmol) were loaded into a Schlenk flask and pumped with vacuum for 10 min. After filling with N_2, degassed acetone (73.0 mL) and a solution of K_2CO_3 (0.122 g, 8.83 mmol) in water were transferred into the flask, respectively. After purging the mixture with N_2 for 20 min, the mixture was refluxed for 24 hours under N_2. After cooing the reaction mixture to room temperature and removing all the solvent by rotary evaporation, CH_2Cl_2 was added. The organic layer was separated, washed with water, dried over $MgSO_4$, filtered, and evaporated to dryness. The crude product was purified by chromatography column with an eluent of CH_2Cl_2/Hexane (6:4) to obtain both the mononuclear and binuclear products.[8] **Pt(Stpip)L2H**: a yellow solid, 0.239 g, 33.5%. HRMS (ESI): m/z: 1027.1770 $[M + H]^+$. Calcd for $C_{52}H_{40}N_3P_2PtS_2$ 1027.1781. **Pt_2(Stpip)$_2$L2**: an orange solid, 0.121 g, 17.0%. HRMS (ESI): m/z: 1668.1795 $[M + H]^+$. Calcd for $C_{76}H_{59}N_4P_4Pt_2S_4$ m/z 1668.1842.

Pt(Stpip)L3H and Pt_2(Stpip)$_2$L3. $L3H_2$ **(**1,4-diazanaphthalene, 0.250 g, 1.09 mmol) was loaded into a Schlenk flask and pumped with vacuum for 10 min. After filling with N_2, degassed acetic acid (75.0 mL) and a solution of K_2PtCl_4 (0.452 g, 1.09 mmol) in water were transferred into the flask, respectively. After purging the mixture with N_2 for 20 min, the mixture was refluxed for 24 hours under N_2. The mixture was cooled to room temperature, filtered, washed sequentially with acetic acid and ethanol, and dried to obtain dichlorobridged intermediate. The dichlorobridged intermediate (0.100 g, 0.220 mmol) and HStpip (0.198 g, 0.440 mmol) were loaded into a Schlenk flask and pumped with vacuum for 10 min. After filling with N_2, degassed acetone (20.0 mL) and a solution of K_2CO_3 (0.0480 g, 3.33 mmol) in water were transferred into the flask, respectively. After purging the mixture with N_2 for 20 min, the mixture was

refluxed for 24 hours under N_2. After cooing the reaction mixture to room temperature and removing all the solvent by rotary evaporation, CH_2Cl_2 was added. The organic layer was separated, washed with water, dried over $MgSO_4$, filtered, and evaporated to dryness. The crude product was purified by column chromatography with an eluent of CH_2Cl_2/Hexane (4:6) to obtain both the mononuclear and binuclear products.[8] **Pt(Stpip)L3H**: an orange solid, 0.0788 g, 30.0%. HRMS (ESI): m/z: 873.0960 $[M + H]^+$. Calcd for $C_{40}H_{30}N_3P_2PtS_2$ m/z 873.0999. **Pt_2(Stpip)$_2$L3**: a red solid, 0.0493 g, 19.5%. HRMS (ESI): m/z: 1515.1064 $[M + H]^+$. Calcd for $C_{64}H_{50}N_4P_4Pt_2S_4$ m/z 1515.1138.

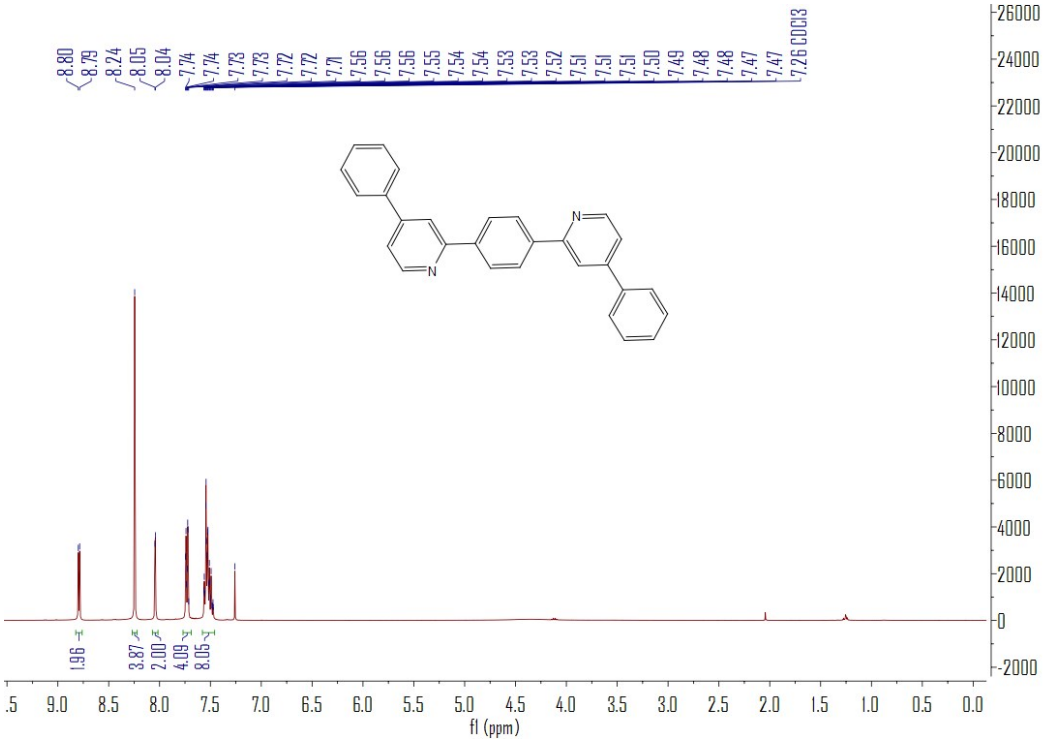

Figure S2. ^{1}H NMR spectrum of **L2H$_2$** ($CDCl_3$).

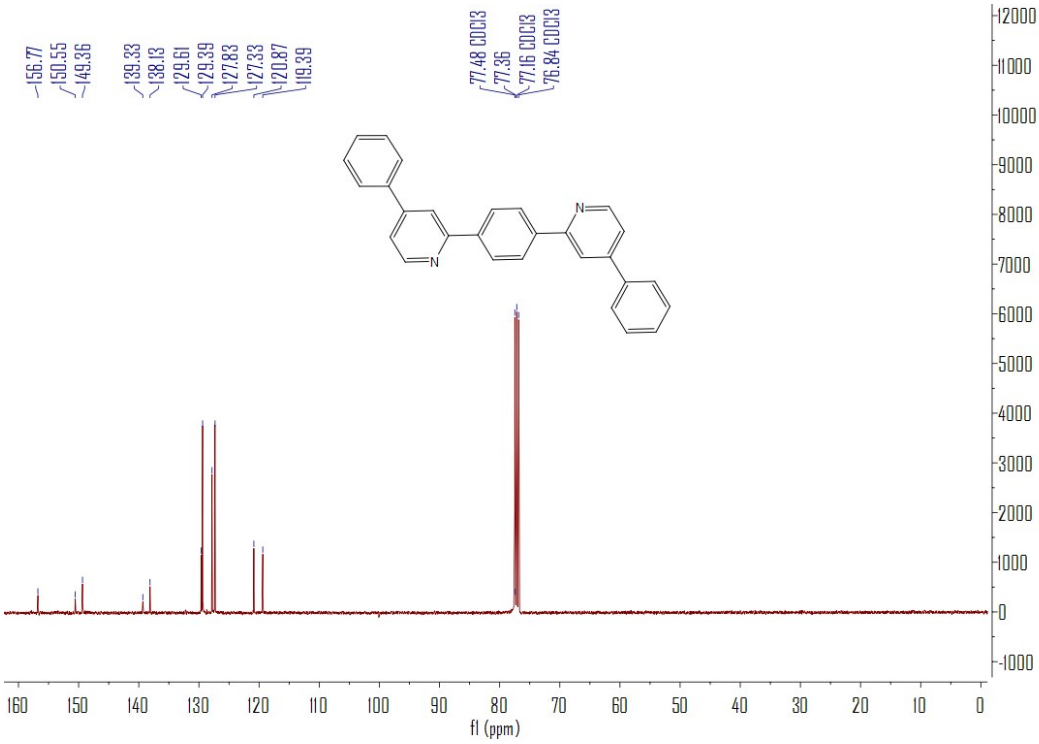

Figure S3. ^{13}C NMR spectrum of **L2H$_2$** ($CDCl_3$).

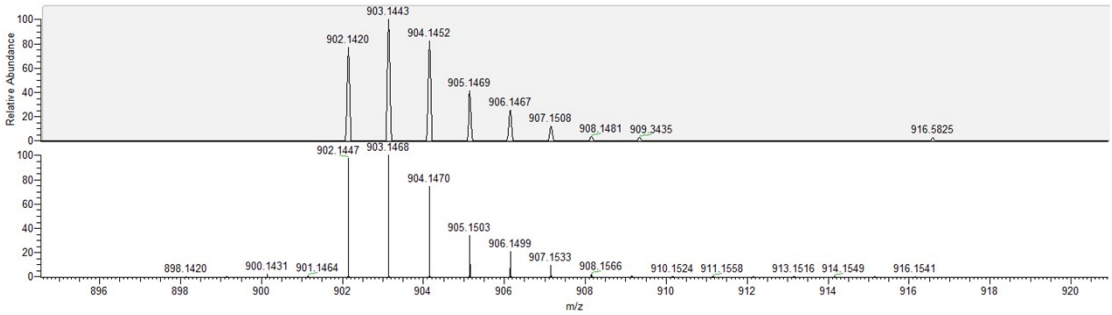

Figure S4. HRMS spectra for **Pt(Stpip)L1H** [M + H]$^+$.

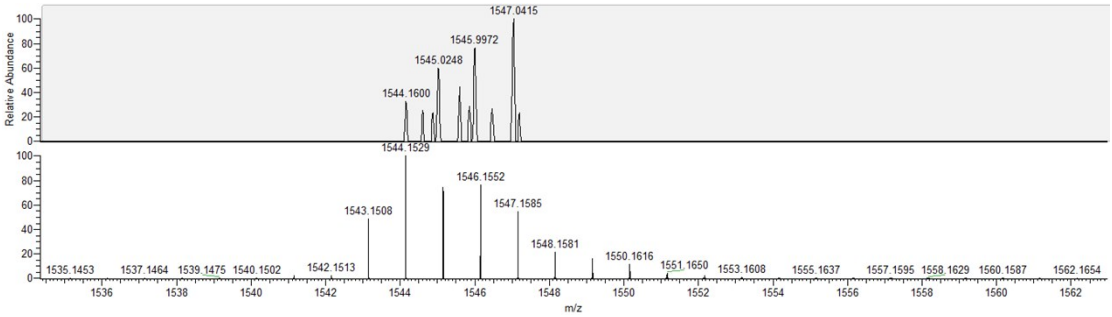

Figure S5. HRMS spectra for **Pt$_2$(Stpip)$_2$L1** [M + H]$^+$.

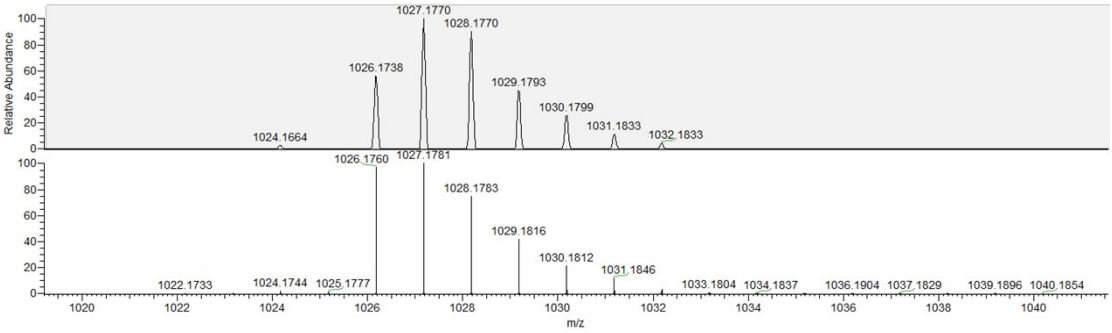

Figure S6. HRMS spectra for **Pt(Stpip)L2H** [M + H]$^+$.

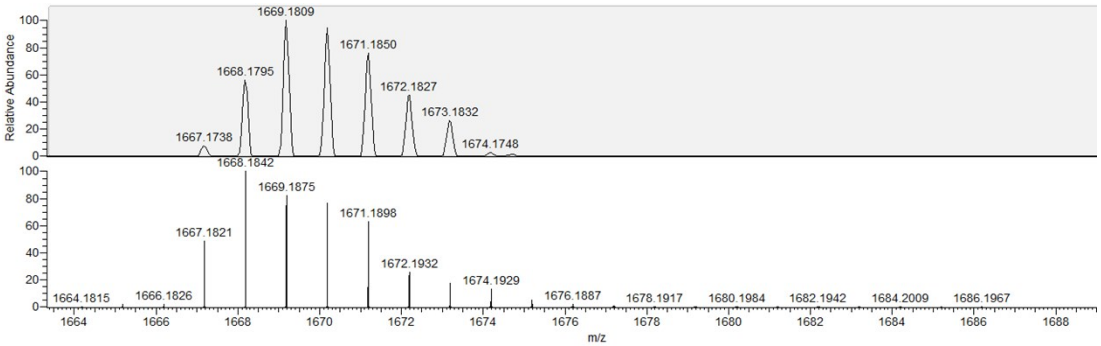

Figure S7. HRMS spectra for **Pt_2(Stpip)$_2$L2** [M + H]$^+$.

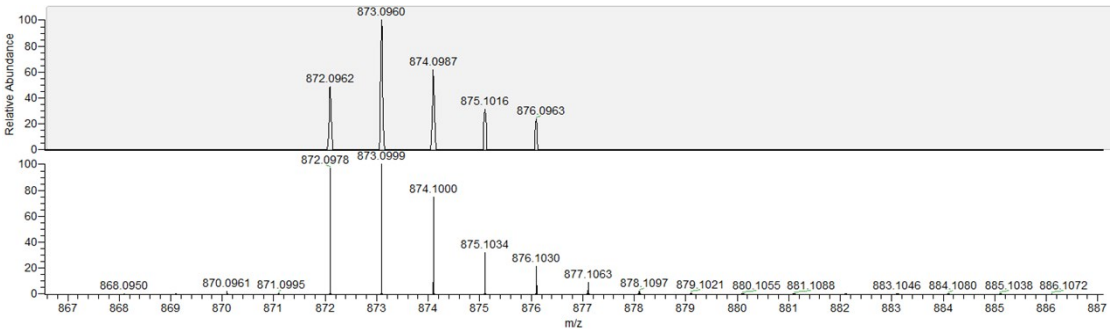

Figure S8. HRMS spectra for **Pt(Stpip)L3H** [M + H]$^+$.

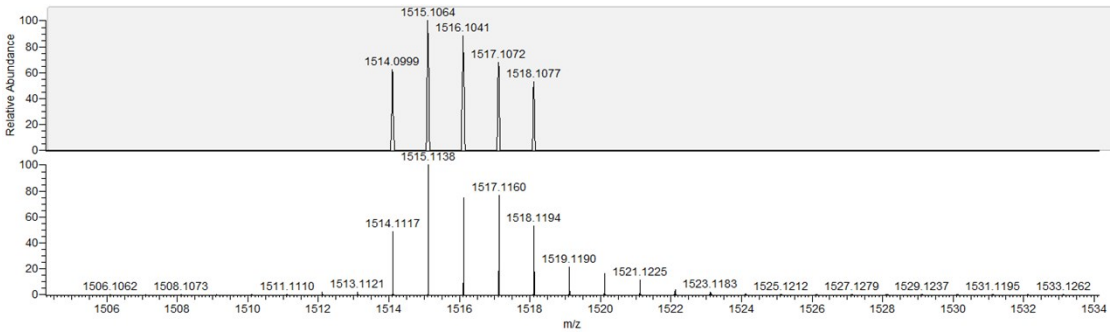

Figure S9. HRMS spectra for **Pt_2(Stpip)$_2$L3** [M + H]$^+$.

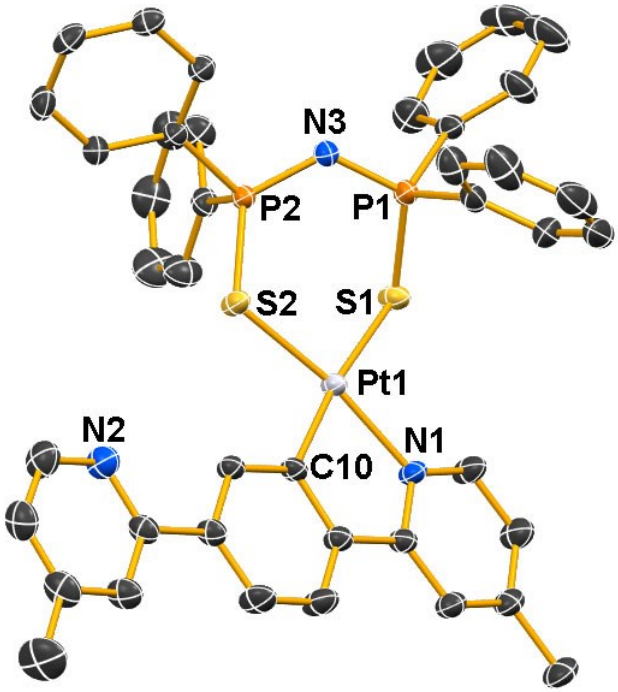

Figure S10. Crystal structure of **Pt(Stpip)L1H**.

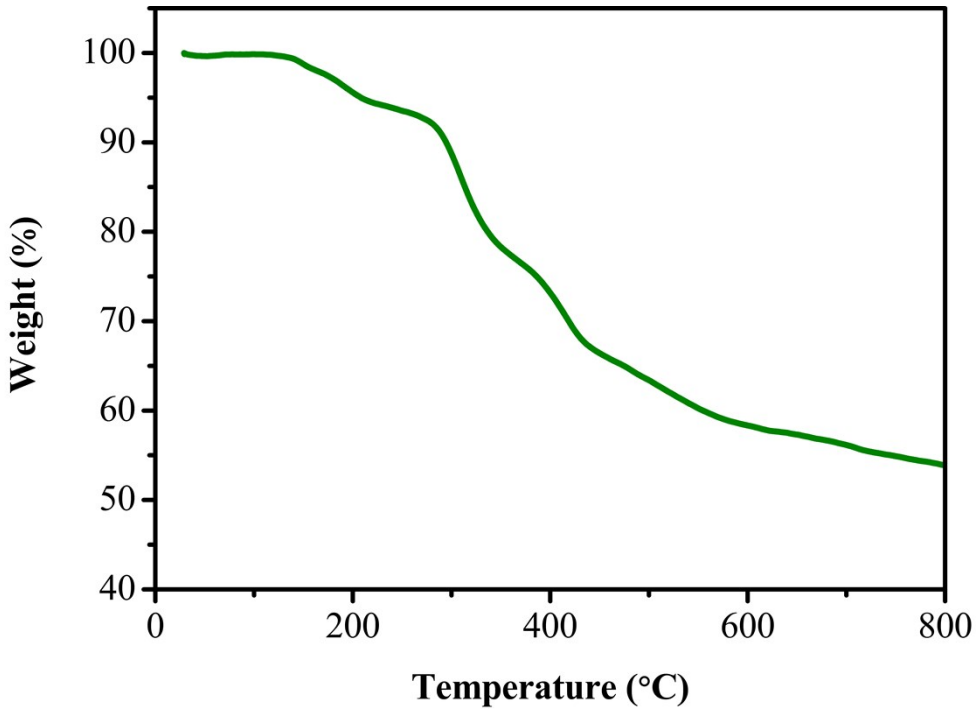

Figure S11. Thermogravimetric analyses of **Pt(Stpip)L1H**.

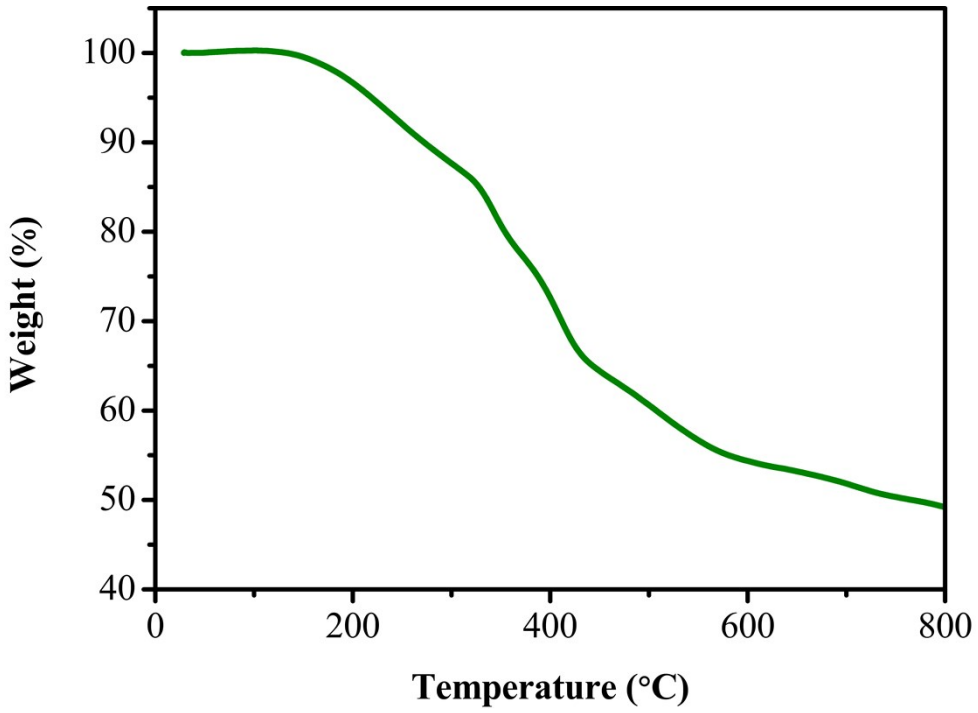

Figure S12. Thermogravimetric analyses of **$Pt_2(Stpip)_2L1$**.

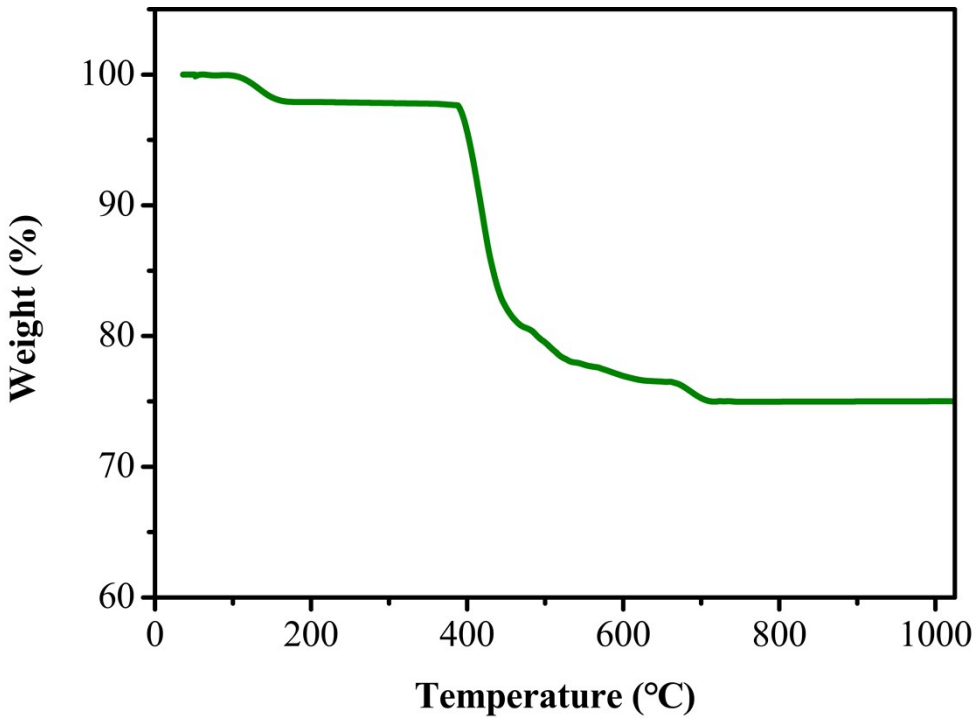

Figure S13. Thermogravimetric analyses of **Pt(Stpip)L2H**.

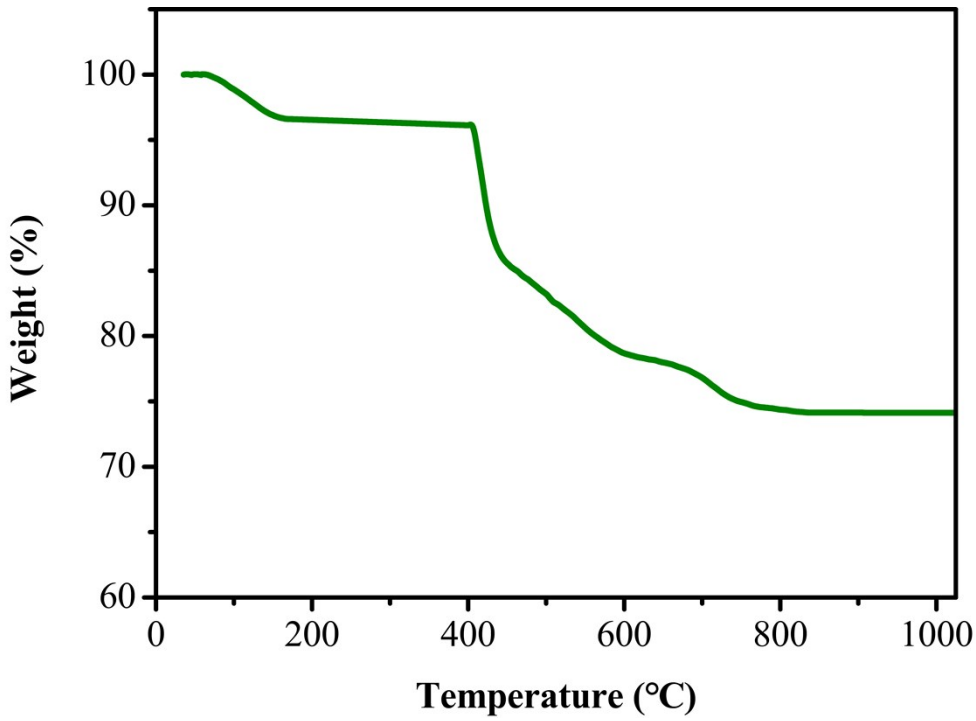

Figure S14. Thermogravimetric analyses of **Pt_2(Stpip)$_2$L2**.

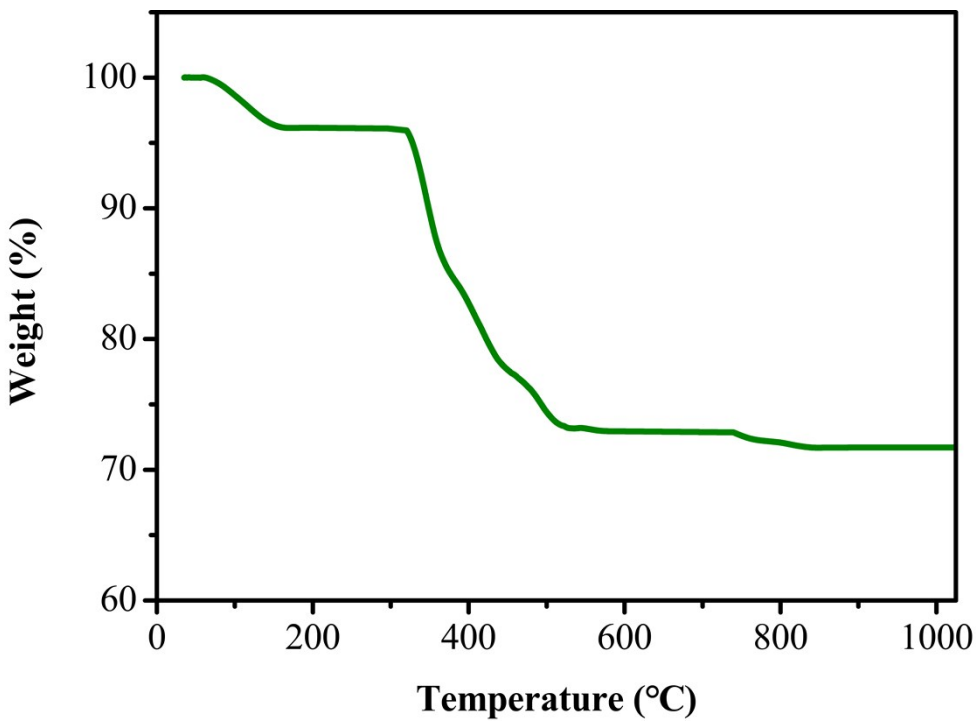

Figure S15. Thermogravimetric analyses of **Pt(Stpip)L3H**.

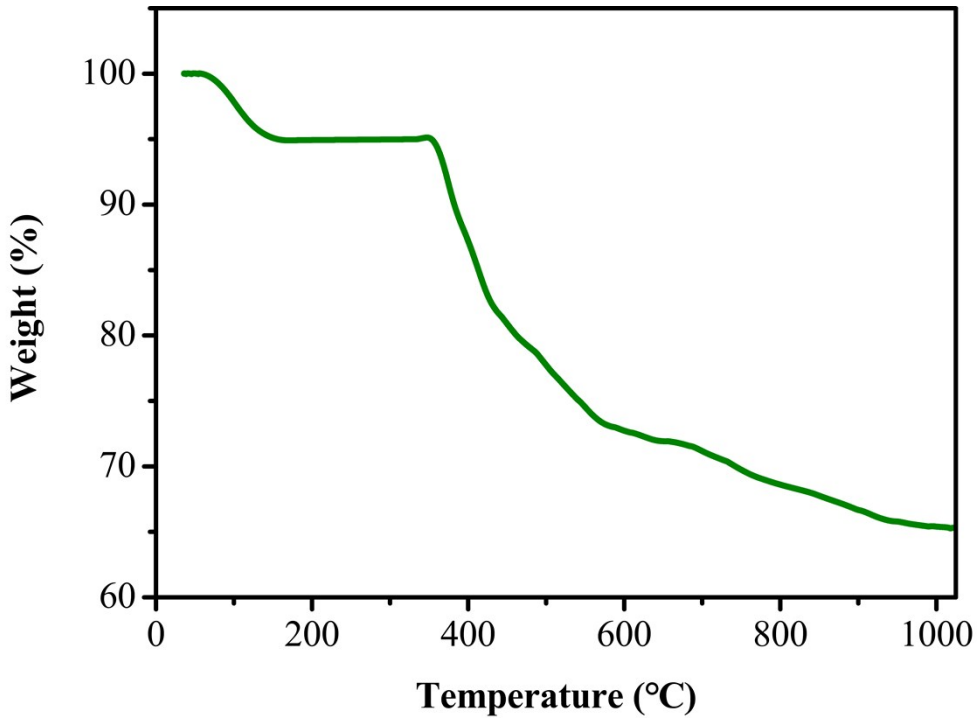

Figure S16. Thermogravimetric analyses of **Pt_2(Stpip)$_2$L3**.

Table S1. Crystal data and structure refinement for **Pt(Stpip)L1H, Pt(Stpip)L2H, $Pt_2(Stpip)_2L2$, Pt(Stpip)L3H and $Pt_2(Stpip)_2L3$**.

	Pt(Stpip)L1H	Pt(Stpip)L2H	$Pt_2(Stpip)_2L2$	Pt(Stpip)L3H	$Pt_2(Stpip)_2L3$
CCDC number	2047596	2047598	2048322	2047600	2047599
Empirical formula	$C_{42}H_{35}N_3P_2PtS_2$	$C_{52}H_{39}N_3P_2PtS_2$	$C_{76}H_{60}N_4P_4Pt_2S_4$	$C_{40}H_{29}N_3P_2PtS_2$	$C_{64}H_{48}N_4P_4Pt_2S_4$
Formula weight	902.91452	1027.01	1671.58	872.84452	1600.29
Temperature/K	296 K	193.01	193.01	296	296.15
Crystal system	triclinic	Monoclinic	Monoclinic	monoclinic	triclinic
Space group	P-1	P21/n	P21/n	I2/a	P-1 (2)
a/Å	10.24020(10)	12.7717(4)	9.7478(7)	20.0870(2)	13.8090(18)
b/Å	11.43860(10)	22.6778(7)	13.3264(10)	20.26000(10)	15.899(2)
c/Å	15.9130(2)	15.4864(5)	30.872(2)	16.73030(10)	16.093(2)
α/°	92.1960(10)	90°	90°	90.00	72.506(2)
β/°	98.4840(10)	97.086(2)	97.353(4)	90.2220(10)	83.851(2)
γ/°	93.7410(10)	90	90	90.00	68.765(2)
Volume/Å3	1837.45(3)	4451.1(2)	3992.2(6)	6808.56(9)	3141.0(7)
z	2	4	2	8	2
ρcalcmg/mm3	1.636	1.533	1.396	1.703	1.692
m/mm-1	9.298	5.397	5.947	10.02	4.813
F(000)	900.0	2048	1648.0	3440.0	1564.0
Crystal size/mm3	0.25 × 0.10 × 0.06	0.1 x 0.08 x 0.06	0.08 x 0.06 x 0.06	0.33 × 0.10 × 0.04	0.18 × 0.12 × 0.11
2Θ range for data collection	2.811 to 77.384°	3.391 to 54.962°	3.146 to 55.506°	3.10 to 67.08°	2.864 to 50.018
Index ranges	-12 ≤ h ≤ 12, -14 ≤ k ≤ 14, -20 ≤ l ≤ 19	-15 ≤ h ≤15, -27 ≤ k ≤26, -18 ≤ l ≤ 18	-11 ≤ h ≤11, -16 ≤ k ≤ 15, -37 ≤ l ≤ 37	-24 ≤ h ≤ 24, -11 ≤ k ≤ 25, -21 ≤ l ≤ 20	-16 ≤ h ≤ 15, -18 ≤ k ≤ 14, -18 ≤ l ≤ 19
Reflections collected	60128	40104	34418	24516	15896
Independent reflections	60128 / 7376 [R(int) = 0.0755]	8463 [R(int) = 0.0451]	7527 [R(int) = 0.1016]	23110 / 6044 [R(int) = 0.0398]	10984 [Rint = 0.0738, Rsigma = 0.1771]
Data/restraints/parameters	7376/0/454	8463/0/541	7527/85/436	6044/0/433	10984/60/731
Goodness-of-fit on F2	1.090	1.038	1.073	1.082	0.974
Final R indexes [I>=2σ (I)]	R1 = 0.0263, wR2 = 0.0664	R_1 = 0.0287, wR_2 = 0.0656	R_1 = 0.0959, wR_2 = 0.2395	R_1 = 0.0282, wR_2=0.0765	R_1 = 0.0661, wR_2 = 0.1369
Final R indexes [all data]	R1 = 0.0266, wR2 = 0.0666	R_1 = 0.0342, wR_2 = 0.0687	R_1 = 0.1416, wR_2 = 0.2725	R_1 = 0.0297, wR_2 = 0.0776	R_1 = 0.1367, wR_2 = 0.1773
Largest diff. peak/hole / e Å-3	0.951/1.270	0.548/-1.299	2.918/-3.067	0.81/-0.58	3.53/-3.02
Flack parameter	n/a	n/a	n/a	n/a	n/a

Table S2. Selected Bond Lengths and Angles for Complexes **Pt(Stpip)L1H, Pt(Stpip)L2H, $Pt_2(Stpip)_2L2$, Pt(Stpip)L3H and $Pt_2(Stpip)_2L3$**.

bond length (Å)			bond angle (deg)
Complex Pt(Stpip)L1H			
Pt(1)-C(10)	2.025(3)	C(10)-Pt(1)-S(2)	89.45(9)
Pt(1)-N(1)	2.061(2)	C(10)-Pt(1)-N(1)	80.72(11)
Pt(1)-S(1)	2.4222(7)	S(2)-Pt(1)-S(1)	98.69(3)
Pt(1)-N(1)	2.061(2)	N(1)-Pt(1)-S(2)	170.08(7)
		N(1)-Pt(1)-S(1)	91.12(7)
		C(10)-Pt(1)-S(1)	171.78(8)
Complex Pt(Stpip)L2H			
Pt(1)-C(10)	1.999(3)	N(1)-Pt(1)-S(1)	96.38(8)
Pt(1)-N(1)	2.047(3)	C(10)-Pt(1)-N(1)	80.31(12)
Pt(1)-S(1)	2.4399(8)	S(2)-Pt(1)-S(1)	90.14(3)
Pt(1)-S(2)	2.2906(8)	N(1)-Pt(1)-S(2)	171.96(8)
		C(10)-Pt(1)-S(1)	176.15(9)
		C(10)-Pt(1)-S(2)	93.00(9)
Complex $Pt_2(Stpip)_2L2$			
Pt(1)-C(1)	2.023(13)	N(2)-Pt(1)-S(2)	91.8(3)
Pt(1)-N(2)	2.116(11)	C(1)-Pt(1)-N(2)	80.9(4)
Pt(1)-S(1)	2.274(4)	S(1)-Pt(1)-S(2)	97.96(13)
Pt(1)-S(2)	2.403(3)	N(2)-Pt(1)-S(1)	169.5(3)
		C(1)-Pt(1)-S(1)	89.6(4)
		C(1)-Pt(1)-S(2)	171.8(4)
Complex Pt(Stpip)L3H			
Pt(1)-C(2)	2.034(4)	N(2)-Pt(1)-S(7)	91.62(9)
Pt(1)-N(2)	2.044(3)	C(2)-Pt(1)-N(2)	81.29(12)
Pt(1)-S(6)	2.3069(10)	S(6)-Pt(1)-S(7)	98.28(3)
Pt(1)-S(7)	2.3926(8)	N(2)-Pt(1)-S(6)	168.38(8)
		C(2)-Pt(1)-S(6)	88.61(9)
		C(2)-Pt(1)-S(7)	172.75(9)
Complex $Pt_2(Stpip)_2L3$			
Pt(1)-C(29)	2.032(8)	N(2)-Pt(1)-S(2)	88.93(19)
Pt(1)-N(2)	2.043(7)	C(29)-Pt(1)-N(2)	81.8(3)
Pt(1)-S(1)	2.286(3)	S(1)-Pt(1)-S(2)	99.70(8)
Pt(1)-S(2)	2.407(2)	N(2)-Pt(1)-S(1)	170.45(19)
		C(29)-Pt(1)-S(1)	89.7(3)
		C(29)-Pt(1)-S(2)	170.5(3)

Symmetry code: i =-x, -y+1, -z+1

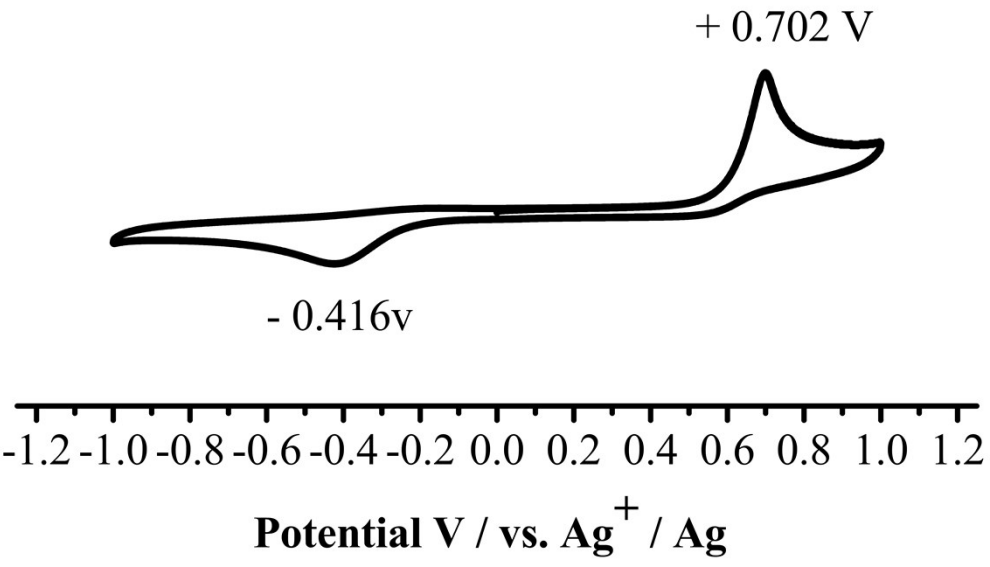

Figure S17. Cyclic voltammetry data of **Pt(Stpip)L1H**.

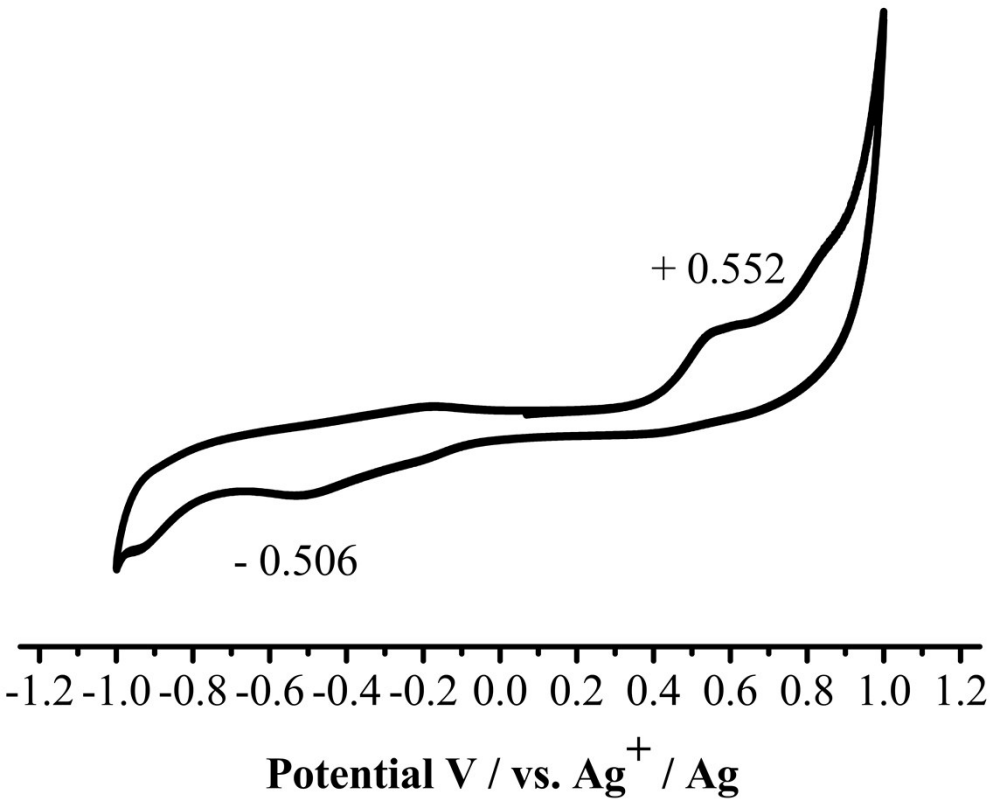

Figure S18. Cyclic voltammetry data of **$Pt_2(Stpip)_2L1$**.

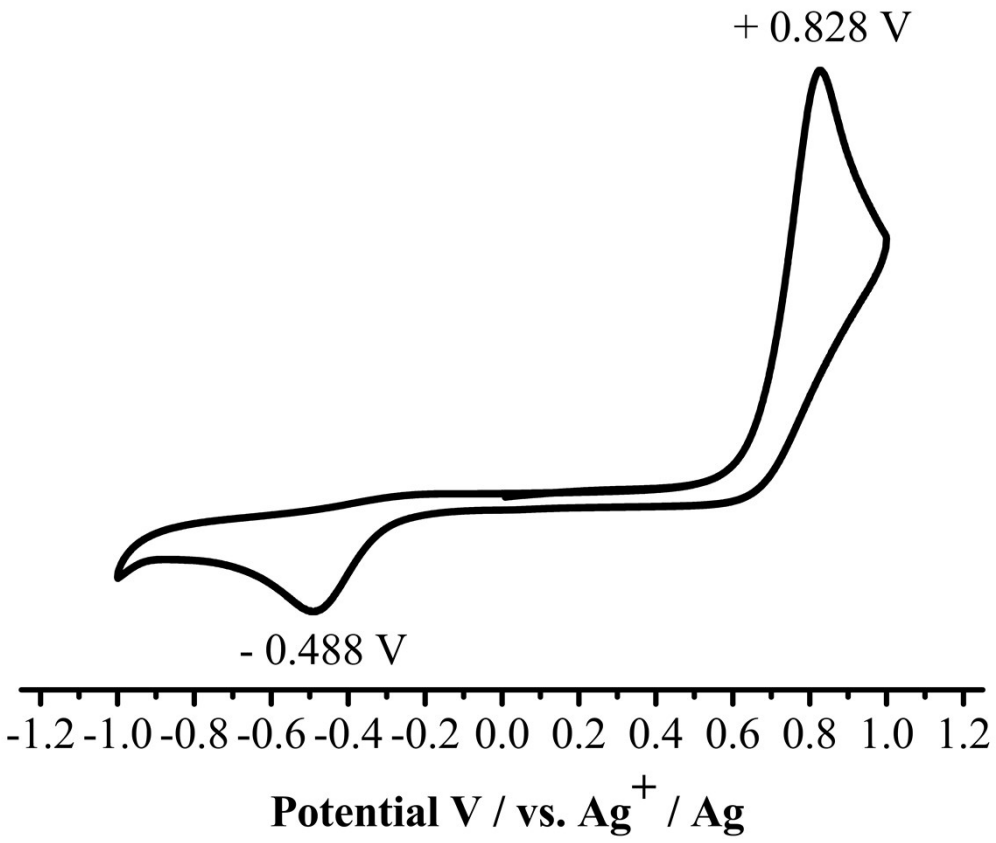

Figure S19. Cyclic voltammetry data of **Pt(Stpip)L2H**.

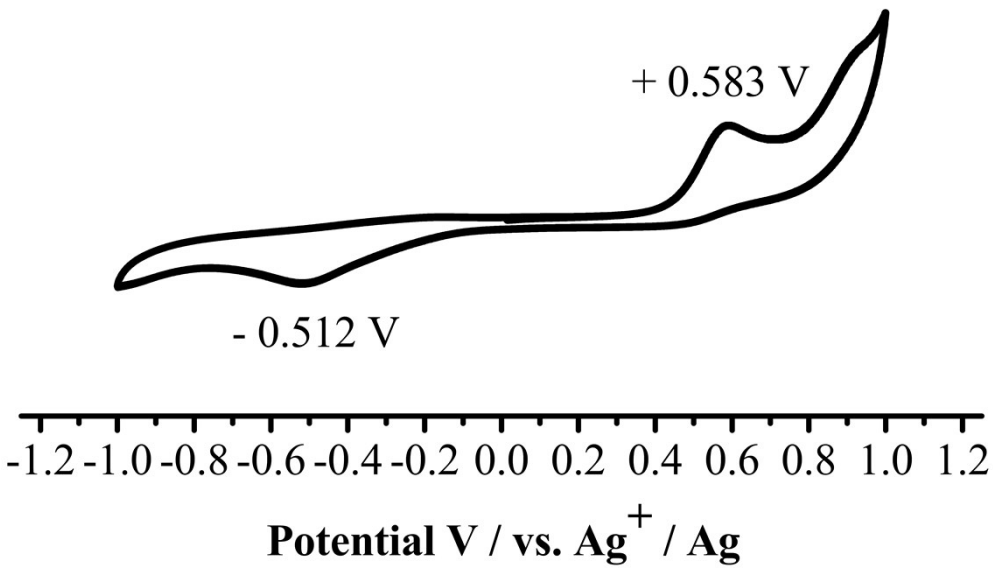

Figure S20. Cyclic voltammetry data of **$Pt_2(Stpip)_2L2$**.

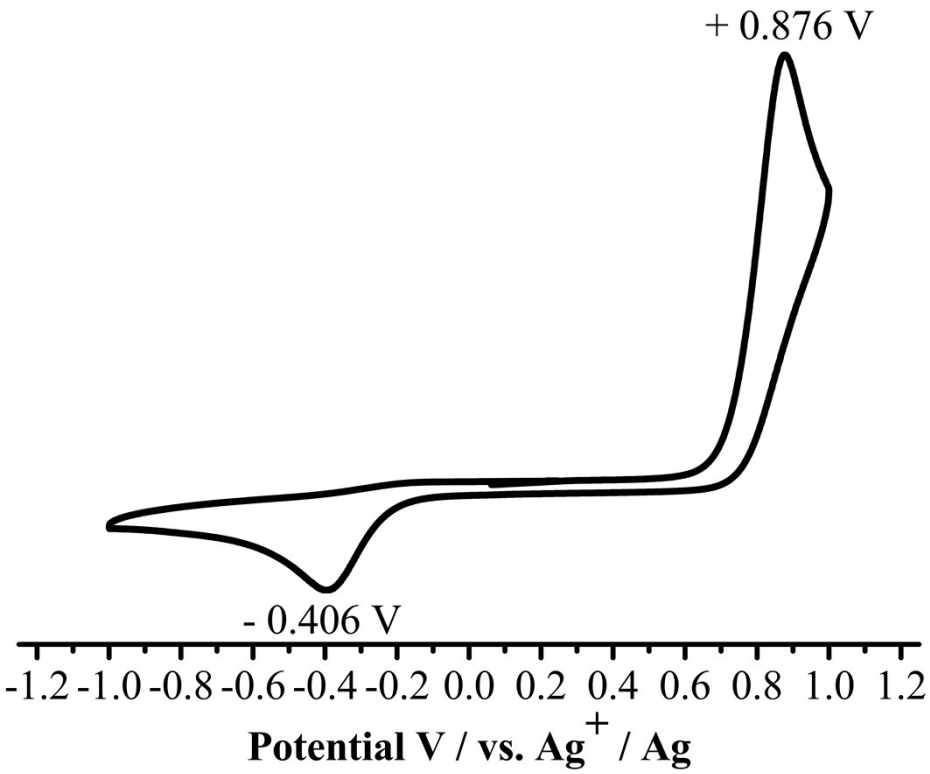

Figure S21. Cyclic voltammetry data of **Pt(Stpip)L3H**.

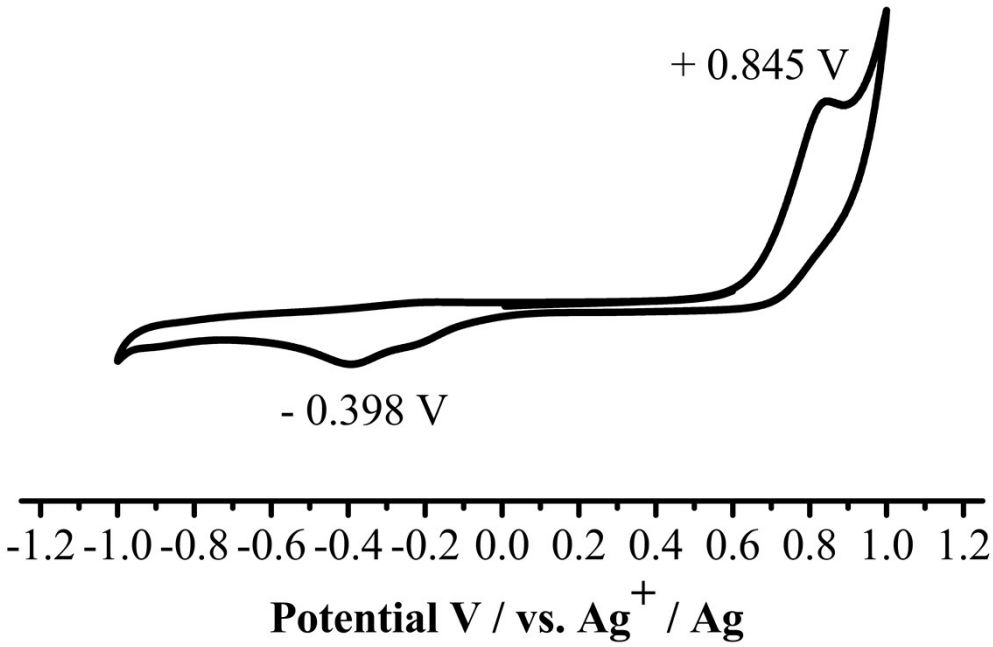

Figure S22. Cyclic voltammetry data of **Pt_2(Stpip)$_2$L3**.

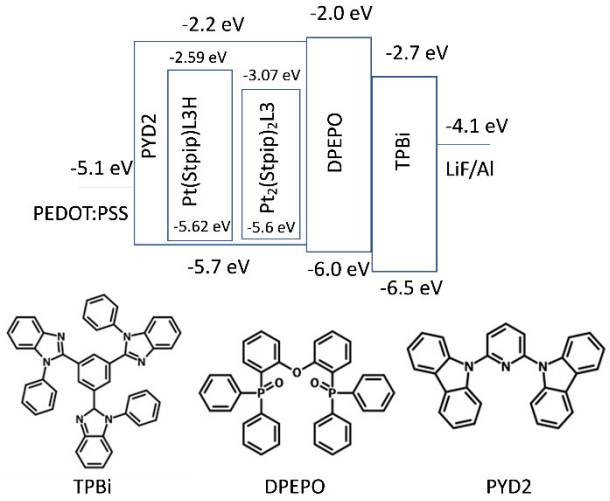

Figure S23. Proposed energy-level diagram of materials used in the OLEDs; chemical structures of organic materials.

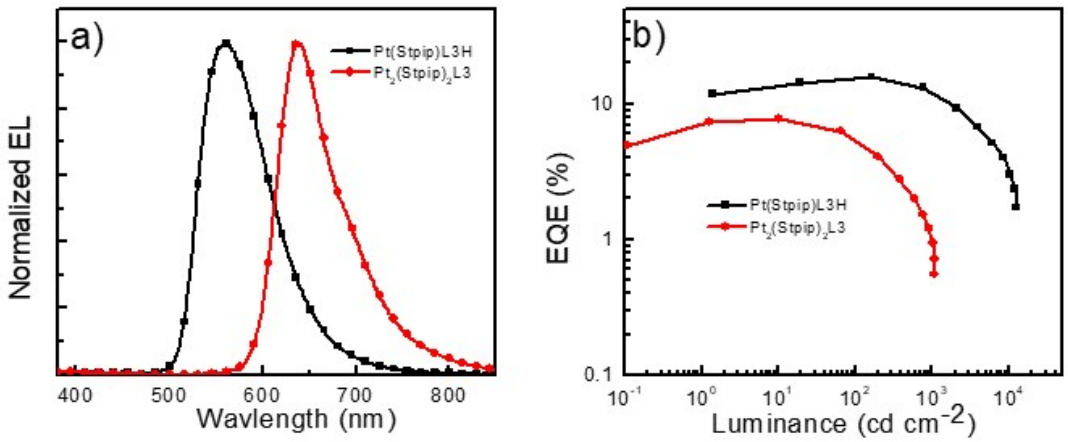

Figure S24. a) Normalized EL spectra and b) EQE-luminance of **Pt(Stpip)L3H** and **Pt_2(Stpip)$_2$L3**-based OLEDs.

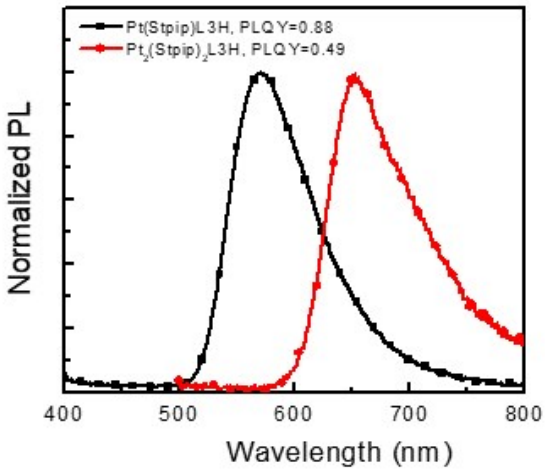

Figure S25. Normalized PL of Pt(Stpip)L3H and Pt2(Stpip)2L3 in PYD2 thin films with a doping concentration of 12 wt%.

Reference

1. Xiao, Z.-Q.; Xu, C.; Li, H.-M.; Han, X.; Wang, Z.-Q.; Fu, W.-J.; Hao, X.-Q.; Song, M.-P., Two fluorescent cyclopalladated arylpyrazine complexes: synthesis, crystal structures and application in the double Suzuki coupling of N-heteroaryl halides with 1,4-benzenediboronic acid. *Transition Metal Chemistry* **2015,** *40* (5), 501-508.
2. Liang, X.; Zhang, F.; Yan, Z. P.; Wu, Z. G.; Zheng, Y.; Cheng, G.; Wang, Y.; Zuo, J. L.; Pan, Y.; Che, C. M., Fast Synthesis of Iridium(III) Complexes Incorporating a Bis(diphenylphorothioyl)amide Ligand for Efficient Pure Green OLEDs. *ACS Appl Mater Interfaces* **2019,** *11* (7), 7184-7191.

3. Xia, J.-C.; Liang, X.; Yan, Z.-P.; Wu, Z.-G.; Zhao, Y.; Zheng, Y.-X.; Zhang, W.-W., Iridium(iii) phosphors with bis(diphenylphorothioyl)amide ligand for efficient green and sky-blue OLEDs with EQE of nearly 28%. *Journal of Materials Chemistry C* **2018,** *6* (33), 9010-9016.
4. Mittal, M.; Jana, A.; Sarkar, S.; Mahadevan, P.; Sapra, S., Size of the Organic Cation Tunes the Band Gap of Colloidal Organolead Bromide Perovskite Nanocrystals. *J Phys Chem Lett* **2016,** *7* (16), 3270-7.
5. Dolomanov, O. V.; Bourhis, L. J.; Gildea, R. J.; Howard, J. A. K.; Puschmann, H., OLEX2: a complete structure solution, refinement and analysis program. *Journal of Applied Crystallography* **2009,** *42* (2), 339-341.
6. Sheldrick, G. M., A short history of SHELX. *Acta Crystallogr A* **2008,** *64* (Pt 1), 112-22.
7. Sheldrick, G. M., Crystal structure refinement with SHELXL. *Acta Crystallogr C Struct Chem* **2015,** *71* (Pt 1), 3-8.
8. Culham, S.; Lanoe, P. H.; Whittle, V. L.; Durrant, M. C.; Williams, J. A.; Kozhevnikov, V. N., Highly luminescent dinuclear platinum(II) complexes incorporating bis-cyclometallating pyrazine-based ligands: a versatile approach to efficient red phosphors. *Inorg Chem* **2013,** *52* (19), 10992-1003.